UNIVERSIDADE DE SÃO PAULO

INSTITUTO DE FÍSICA
CAIXA POSTAL 20516
01452-990 SÃO PAULO - SP
BRASIL

PUBLICAÇÕES

IFUSP/P-1113

OXYGEN VACANCY CENTERS IN SILICATES. I. OPTICAL ABSORPTION SPECTRA

Sadao Isotani, Waldemar Bonveti Jr., Kazunori Watari, Akiyoshi Mizukami, Ana Regina Blak, Amando Siuiti Ito
Instituto de Física, Universidade de São Paulo

Antonio Roberto Pereira Leite Albuquerque
Escola Politécnica, Universidade de São Paulo

Maio/1994

OXYGEN VACANCY CENTERS IN SILICATES. I. OPTICAL ABSORPTION SPECTRA

Sadao Isotani, Waldemar Bonventi Jr., Kazunori Watari, Akiyoshi Mizukami, Ana Regina Blak, Amando Siuiti Ito
Instituto de Física, Universidade de São Paulo
C.P. 20.516, 01452-990, São Paulo, SP, Brasil

and

Antonio Roberto Pereira Leite Albuquerque
Escola Politécnica, Universidade de São Paulo

Key words: Beryl, Vacancy, Absorption

PACS–90: 78.50. Ec

ABSTRACT

The oxygen vacancy UV optical absorption spectra have been investigated by spectral decomposition analysis in spodumene, topaz and beryl. The bar-graph of the spectral decomposition showed a lower energy triplet and a higher energy singlet. It have not been seen zany associated EPR lines. Discussions support the attribution of the UV OA spectra to F centers (oxygen vacancy containing two trapped electrons). A single electron calculation assuming a potential well due to the charge polarization produced by the absence of oxygen atom at the site of O^{2-} ion, shows the split of $2s$ (higher energy) and $2p$ (lower energy) levels. The group symmetry analysis for a lower symmetry potential well show that the $2p$ levels also split in three level. Therefore the UV lines are attributed to $1^1S_0 \rightarrow 2^1P_1$ (triplet) and $1^1S_0 \rightarrow 2^1S_0$ (singlet) multielectronic transitions.

I. INTRODUCTION

Oxygen vacancies are the most extensively studied intrinsic and radiation induced defects in silicon dioxide materials.[1]

Oxygen vacancy is a kind of intrinsic defect that probably has its origin in the crystal growth. Such defect is generally stable at room temperature and is capable of moving to the surface at slightly higher temperatures.[2] The occurrence of intrinsic point defects, at any temperature is demanded from thermodynamics.[1] The long life of the crystal and its exposure during these years to a nearly constant oxygen atmosphere pressure, guarantee the thermodynamical equilibrium between concentration of oxygen vacancy centers and the oxygen atmosphere.

In processes of ternary oxides reduction in perovskite and related families[1,3] both F (an oxygen vacancy containing two trapped electrons) and F^+ (an oxygen vacancy containing one trapped electron) centers are formed. For $LiNbO_3$ the electrical conductivity dependence on the oxygen partial pressure suggests that F^+ centers are more stable than F centers. In contrast, for $SrTiO_3$ and $BaTiO_3$ oxygen vacancies are not stable traps for single electrons.

Color centers studies in sapphire, during the last thirty years, indicate that F and F^+ centers are always present and that the dominant peak in the OA spectra is centered in approximately 6 eV.[1,4–7]

The research of the defect structure of both quartz and its amorphous relative silica, is associated to the development of optical and electronic devices which are able to perform reliably in high background radiation environments.[8] Examples of such devices are MOS devices,[9–12] silica fibre light guides[13–15] and quartz crystal oscillators.[16,17]

The most extensively studied intrinsic and radiation induced defects in quartz are those associated with oxygen vacancies. They have been found in all forms of SiO_2

including crystalline α-quartz,[18–23] amorphous silica[18,24–28] and thin SiO_2 films in MOS devices.[29,30] An optical absorption band at 6.2 ev in crystalline quartz has been associated with the E_1' spin resonance line.[31,32] The model for this center is that of an (oxygen)$^-$ vacancy between two adjacent SiO_3 cluster, one planar similar to molecular SO_3 without dangling bond and other analogous to pyramidal SO_3 with an extra electron.[22,33] The E_2' and E_4' EPR lines have been associated with oxygen vacancy which attracted proton and hydride ion,[23,31,34] respectively.

Two main bands at around 5.6 ev and 7.6 ev , have been observed in the optical absorption spectra of SiO_2. Impurities of Al also show small effect on these bands.[26] The two bands increases by neutron irradiation,[19] showing that it is produced by dislocation of atoms. Following similar arguments for the attribution of E' centers, the two bands have been attributed to two different oxidation states of oxygen vacancy center.

The objective of this work is the analysis of the UV optical absorption spectra of oxygen vacancy centers in silicates by spectral decomposition analysis, electronic calculation using a charge polarization model and a group symmetry analysis. The aim is to obtain a better understanding of oxygen vacancy centers structure in oxides.

II. EXPERIMENTAL DETAILS AND MATERIALS

Spodumene is a silicate mineral whose chemical composition is $LiAlSi_2O_6$. Color in spodumene is associated with impurity ions present in the crystal structure.[35–38] Descriptions of color changes in spodumene induced by irradiation or by heating were reported elsewhere. The color of lilac spodumene is changed to dark by X-ray and γ-ray irradiation. The origin of the color change has been the subject of discussion.

The lilac spodumene crystal used in this study was described elsewhere.[39] The X-ray fluorescence analysis concentrations of transition-metal impurities in the lilac spodumene

sample was made using a Rigaku-Denki X-ray spectrometer.[40] The impurity concentrations are 460 ± 10 ppm for Mn, 165 ± 8 ppm for Fe and 90 ± 20 ppm for Cr. Slices of 0.5 to 0.8 mm thickness were cut, with the c axis perpendicular to the plane of the slice.

Topaz is a silicate class mineral of the "Al_2SiO_5" group, with chemical formula $Al_2(F,OH)_2SiO_4$. It occurs commonly in high temperature veins, probably formed by igneous intrusions in the presence of fluorine and water vapour.

The topaz crystal used in this study was obtained in the region around Governador Valadares, Minas Gerais. Different of other topaz crystals described in literature[41,42], this sample does not develop blue color by irradiation. The irradiation induces a brown color, which by heating above $100°C$ is annealed. Slices of about 0.5 mm thickness were obtained by cleavage.

Beryl is a cyclosilicate with chemical formula $Be_3Al_2Si_6O_{18}$. It belongs to the hexagonal system, and the unit cell contains two formula units. Beryl belongs to space group P6/mmcc. The Si_6O_{18} rings form structural channels parallel to the unique crystallographic axis.

The beryl crystal used in this study was also obtained in the region around Governador Valadares, Minas Gerais. Slices of 0.3 to 1.0 mm thickness were cut, with the c axis perpendicular to the plane of the slice.

A Carl-Zeiss DMR 21 spectrophotometer was used for the optical absorption measurements. All spectra were obtained at room temperature. The EPR spectra were obtained using a Varian x-band type spectrometer using a TE_{102} rectangular cavity.

The sample was irradiated with γ-rays from a ^{60}Co source ($\sim 4 \times 10^5$ Ci) at EMBRARAD S.A. The dose was monitored by three means: a ceric-cerous dosimetric system, AECL red acrylic dosimetric system and UKAEA red perspex dosimeter.

Thermal treatments were carried out in air. The stability of the furnace with a useful

volume $10 \times 12 \times 15$ cm was improved to $1°C$ by filling it with brick refractary materials and two parallel metallic plates. The temperature was measured using a chromel-alumel thermocouple, with one junction at $0°C$ with an ECB xt-recorder and Keithley 160B digital multimeter. The slices to be treated were placed between previously heated metallic plates.

III. RESULTS

a. Spodumene

Lilac spodumene presents absorption bands at 11500 (1.42), 18600 (2.31) and $\sim$ 22000 cm^{-1} (2.73 ev). Irradiated dark green spodumene presents new absorption bands at 10500 (1.30), 15600 (1.93) and $\sim$ 21500 cm^{-1} (2.67 ev). Detailed analysis of the decay kinetics and curve-dose showed that both sets of bands are due to a couple of different color centers, say Mn^{3+} and L and G sites.[38,39]

Figure 1 shows the optical absorption spectrum of annealed spodumene. A wide absorption band at 38300 cm^{-1}, over a strongly increasing UV band edge, has been observed.

INSERT FIGURE 1

The analysis of the line-shape of the spectrum may help to determine roughly the optical band gap energy and the number and characteristics of the absorption bands. To perform this analysis, we need first to determine the line-shape of the absorption bands. The breadth of a line may have its origin from several sources. The band is composed of narrow subbands, and each individual width arises from the uncertainty principle and the dispersion of normal modes. The envelope curve arises from the displacement of the normal modes which occur during an optical transition. The overall shape can be

approximated by several types of well-known line-shapes: Gaussian, Lorentzian, double Gaussian, Pekarian or a combination of these lines. Markham[43] has shown rigorously that for potential energies of ground and excited states with different minima, the shape gives a symmetrical curve at high temperature. Markham has also shown that at room temperature this condition is usually satisfied. Thus, a symmetrical line-shape was assumed for modeling the room-temperature spectra. Also, from approximate evaluation, Markham has shown that the high-temperature absorption should be Gaussian. Therefore, a Gaussian line-shape was assumed for modeling the room-temperature spectra.

The UV band-edge is expected to show a sharp increase reaching a step from which it depends on the density of states of the valence and conduction bands in a complicated way. However, the broadening of the UV band-edge absorption below the step shows their dependence on the uncertainty principle and the dispersion of normal modes. Thus, a Gaussian line shape was assumed for modeling the increasing part of the UV band edge.

The fit was performed by sucessive subtraction of proeminent lines and stopping the recursion when the remaining data is of the order of the measurement error. Also, the data resulting from subtraction, within the measurement error precision, was restricted to positive values.

A good fit was obtained for the sum of three Gaussian lines ($i = 1, 2, 3$) and one Gaussian UV band-edge ($i = 4$):

$$B(\overline{\nu}) = \sum_{i=1}^{4} a_i \exp\left(-(\ln 2)(\overline{\nu} - \overline{\nu}_{oi})^2 / (\Delta\overline{\nu}_i)^2\right) \quad , \qquad (1)$$

where $\overline{\nu}$ is the wavenumber, $\overline{\nu}_{oi}$ is the wavenumber of the i-th line at the maximum, a_i is a constant that expresses the intensity of the i-th line and $\Delta\overline{\nu}_i$ expresses the value of the line width of the i-th line.

The best fit parameters are shown in Table I. Within the trace error the adjusted

curve agrees fairly with the experimental one.

INSERT TABLE I

The decomposition of the spectra in terms of gaussians can be used when the observed bands issue from internal transitions and are not connected with free-to-bond states transitions. The observed optical absorption bands looks to be localized very near the band-edge and it is not garanted that they do correspond to such internal electronic transitions. In this way we analysed the spectra in terms of Lorentzian series. It results that the number of lines remains the same with similar values for $\overline{\nu}_{0i}$ and $\Delta\overline{\nu}_i$. So, we conclude that the method of deconvolution of the absorption bands is good enough to produce meaningful number of lines. Then, for the sake of simplicity, we use Gaussian series independent of the nature of transitions.

INSERT FIGURE 2

Figure 2 shows the difference spectrum in the UV region, of a slice of lilac spodumene and a slice of bleached spodumene. The difference of thickness between these slices, although small, does not avoid the contribution of the background represented by the spectrum of the annealed sample. Thus the difference spectrum was fit together with the background (equation 1) and the sum of six Gaussian lines:

$$D(\overline{\nu}) = \sum_{i=5}^{10} a_i \exp\left(-(\ln 2)(\overline{\nu} - \overline{\nu}_{oi})^2 / (\Delta\overline{\nu}_i)^2\right) + 0.21\, B(\overline{\nu}) - 0.05 \quad . \qquad (2)$$

The adjusted parameters are shown in Table I.

Figure 3 shows the optical absorption spectra for γ-irradiated spodumene.

INSERT FIGURE 3

Three bands, a, c and f were analysed including the bands at 15600 cm^{-1} and 18600 cm^{-1}. The spectra were fit with the background (equation 1) and the sum of eight Gaussian lines:

$$F(\overline{\nu}) = \sum_{i=5}^{12} a_i \exp\left(-(\ln 2)(\overline{\nu} - \overline{\nu}_{oi})^2 / (\Delta\overline{\nu}_i)^2\right) + 0.81\, B(\overline{\nu}) \quad . \qquad (3)$$

The adjusted parameters are shown in Table I. The line at 18600 cm^{-1} remain constant. The lines at 15600, 21000, 43700 and 47500 cm^{-1} show a relation between the intensities of 2 : 1 : 18 : 10, respectively, for all curves a, c and f. The lines at 28800 and 40600 cm^{-1} show a relation between the intensities of 2.7 : 1, respectively, for all curves a, c and f. The lines at 33400 cm^1 show a intensity variation different of other lines.

b. Topaz

The irradiation coloration is not always uniform and some patchiness and banding is observed. All of the reddish to brown irradiation induced color were loss on heating at 200°C for some minutes, turning colorless or blue, agreeing with the previous reports.[41,42]

Here, we examined a sample which does not turn blue. Figure 4 shows the optical absorption spectra of irradiated and annealed samples at 200°C and 600°C.

INSERT FIGURE 4

A good fit was obtained for the sum of 7 Gaussian lines and one Gaussian UV band-edge. The best fit parameters are shown in Table II.

INSERT TABLE II

c. Beryl

Here, we examined a pink color beryl crystal. Figure 5 shows the optical absorption of natural sample and after 55 h annealing at 750°C.

INSERT FIGURE 5

A good fit was obtained for the sum of 4 Gaussian lines and one Gaussian UV band-edge. The best fit parameters are shown in Table III.

INSERT TABLE III

IV. ANALYSIS OF THE RESULTS

Among the several lines observed in the spodumene, topaz and beryl we find a group of four lines which showed to be resistant on heating below 600°C and irradiation with ionizing radiation. Figure 6 shows the bar-graph of the lines.

INSERT FIGURE 6

Previous reports on sapphire and quartz attributed the UV band at about $40,000 \sim 50,000 cm^{-1}$ to F and F^+ electronic absorption centers. A remarkable similitude between these bands and those observed here, lead us to attribute the UV bands of spodumene, beryl and quartz to F and F^+ centers. The UV bands are not associated with any EPR signal. Therefore we conclude that these heat resistant lines are electronic absorption from F centers.

Also, we include in Figure 6, for comparison, the well studied UV quartz lines assigned to E' centers. The best fit parameters for Gaussian lines are shown in Table IV, from data obtained from Sigel.[26]

An inspection of heat resistant lines, show a group of three lines at around $40,000 cm^{-1}$ (T-lines) and a single line (S-line).

V. A THEORETICAL MODELING OF F CENTER IN OXIDES

The oxygen ion in the lattice structure has nominal charge $-2e$. The absence of an oxygen ion induces changes in the charge distribution around the vacancy. Here, for the sake of simplicity, we assume that this effect gives rise to a polarized charge distribution around an imaginary surface of radius R, which substitute the oxygen ion. This charge distribution gives rise, by turn, to an electric potential energy of the form:

$$V(r) = \begin{cases} \dfrac{-Ze^2}{R} & \text{for} \quad 0 < r < R \quad , \\ \dfrac{-Ze^2}{r} & \text{for} \quad r > R \quad , \end{cases} \tag{4}$$

where Z is the effective charge at the polarized surface.

The calculation of the one electron energy levels using the potential, is shown in Figure 7.

INSERT FIGURE 7

The calculation of the radial part of the Schroedinger equation with the potential given above have been done using the Numerov's method.[44] The remarkable feature is that the presence of the polarization surface split the energy level with different values of ℓ, and the energy levels being smaller for smaller ℓ values.

In quartz, each oxygen links two SiO_4 tetrahedra. In spodumene, two of four oxygen of the SiO_4 tetrahedra links two SiO_4 tetrahedra and the other two are bonded to Li and Al atom through ionic bonds. In topaz, also, two oxygen of SiO_4 tetrahedra links two SiO_4 tetrahedra and two oxygen are bonded to Al. In beryl, two oxygen of the SiO_4 tetrahedra links two SiO_4 tetrahedra and the other two are bonded to Be and Al. In all cases, the site symmetry of the oxygen site is very low, belonging to symmetry group C_{1v} (topaz), C_{2v} (quartz, beryl channel and oxygen belonging to two

SiO_4 tetrahedra of spodumene) and C_1 (Si–O–(Al,B) bonds of beryl and Si–O–(Al,Li) bonds of spodumene).

The orbital $1s$ is not split in any case of crystal field distortion.

The orbital $2p$ can split. Using the standard procedures[45] we evaluate the group representation of the $2p$ orbital in the site symmetry of the oxygen atoms, shown in Table V. We see that all cases, $2p$ orbital degeneracy is completely removed.

INSERT TABLE V

At first order approximation, by neglecting the electron-electron repulsion energy, the electronic transition from the multielectronic levels 1^1S_0 and 2^1P_1 can be assumed to be similar to the monoelectronic transition from $1s$ to $2p$ levels.

Then the 1^1S_0 and 2^1S_0 levels are not split by crystal field distortion. Otherwise, the 2^1P_1 level is split in three lines for the symmetries of all crystals considered here.

Therefore the $1^1S_0 \rightarrow 2^1S_0$ multielectronic transition is not split and the $1^1S_0 \rightarrow 2^1P_1$ multielectronic transition is split in three lines. Also, from figure 6, we show that the splitted $1^1S_0 \rightarrow 2^1P_1$ transitions have smaller energy than the $1^1S_0 \rightarrow 2^1S_0$ transition.

For spodumene, assuming $Z = 1.3$[46] and that transition energy is about 4.5 eV we found from figure 7 that the value of the surface polarization radius, R, is about 0.8 Å, which is consistent with the radius of O^{2-} of about 1.2 Å. The smaller polarization radius value, probably, show the importance of the electron-electron repulsion energy in the calculation of the multielectronic states, because we are dealing with a very compact orbital $1s$.

VI. CONCLUSIONS

The spectral decomposition analysis, applied to the optical absorption spectra in the

ultraviolet range of quartz, spodumene, beryl and topaz, led to conclusions which can be summarized as below:

(a) The bar-graph lines show a triplet around $40,000\text{cm}^{-1}$ and a singlet at around $60,000\text{cm}^{-1}$, which are stable on heating up to 600°C.

(b) These stable lines were attributed to F centers.

(c) Oxygen vacancy polarized charge potential single electron calculation showed the splitting of the $2s$ levels

(d) The $2p$ level has smaller energy than the $1s$ level.

(e) A group representation analysis show that the multielectronic states $1S_0$ and $2S_0$ are not split by the crystal field of the crystals and that the 2^1P_1 is split in three levels.

Therefore, we conclude that the observed triplet around $40,000\text{cm}^{-1}$ is due to $1^1S_0 \rightarrow 2^1P_1$ multielectronic transition splitted by the crystal field and that the singlet around $60,000\text{cm}^{-1}$ is due to $1^1S_0 \rightarrow 2^1S_0$ transition.

ACKOWLEDGEMENTS

This work was supported by grants of CNPq, RHAE from SCT, FAPESP and FINEP.

REFERENCES

[1] F. Agullo-Lopez, C.R.A. Catlow, P.D. Townsend, "Point Defects in Materials", Academic Press, London, San Diego (1988).

[2] D.S. Goldman, G.R. Rossman and K.M. Parkin, *Phys. Chem. Minerals* **3**, 225 (1978).

[3] G.H. Kinchin and R.S. Pease, *Rep. Prog. Phys.* **18**, 1 (1955).

[4] P.W. Levy and G.J. Dienes, Report on Conference on Defects in Crystalline Solids, Bristol, Physical Society, London, p. 256 (1955).

[5] E.W.J. Mitchell, J.D. Rigden and P.D. Townsend, *Philos. Mag.* **5**, 1013 (1960).

[6] P.W. Levy, *Phys. Rev.* **123**, 1226 (1961); *Discuss. Faraday Soc.* **31**, 118 (1961).

[7] J.H. Crawford, *Semicond. Insul.* **5**, 599 (1983).

[8] S.W.S. Mckeever, *Radiation Protection Dosimetry* **8**, 81 (1984).

[9] J.R. Srour, O.L. Curtis and K.Y. Chiu, *I.E.E.E. Trans. Nucl. Sci.* **NS-21**, 173 (1974).

[10] O.L. Curtis, J.R. Srour and K.Y. Chiu, *I.E.E.E. Trans. Nucl. Sci.* **NS-22**, 174 (1975).

[11] J.R. Srour, S. Othmer, O.L. Curtis and K.Y. Chiu, *I.E.E.E. Trans. Nucl. Sci.* **NS-23**, 1513 (1976).

[12] J. Van Turnhout and A.H. Van Rheener, *J. Electrostat.* **3**, 213 (1977).

[13] E.M. Dianov, L.S. Korienko, E.P. Nikitin, A.O. Rybattovskii and P.V. Chirnov, *Sov. J. Glass Phys. and Chem.* **6**, 239 (1980).

[14] G.H. Sigel, E.J. Friebele, M.J. Marrone and M.E. Gingerich, *I.E.E.E. Trans. Nucl. Sci.* **NS-28**, 4095 (1981).

[15] G.H. Sigel and M.J. Marrone, *J. Non-Cryst. Solids* **45**, 235 (1981).

[16] J.C. King and H.H. Sander, *Radiat. Effects* **26**, 203 (1975).

[17] R.E. Paradysz and W.L. Smith, *Radiat. Effects* **26**, 213 (1975).

[18] E. Lell, N.J. Kriedl and J.R. Hensler, *Progr. Ceram. Soc.* **4**, 3–40 (1966).

[19] E.W.J. Mitchell and E.G.S. Paige, *Phil. Mag.* **1**, 1085–115 (1956).

[20] R.A. Weeks, *Phys. Rev.* **130**, 570–6 (1963).

[21] R.H. Silsbee, *J. Appl. Phys.* **32**, 1453–62 (1961).

[22] F.J. Figel, W.B. Fowler and L.K. Yip, *Solid State Commun.* **14**, 225–9 (1974).

[23] J. Isoya, J.A. Weil and O.L.E. Halliburton, *J. Appl. Phys.* **74**, 5436–48 (1981).

[24] E.M. Dianov, L.S. Korienko, E.P. Nikitin, A.O. Rybattovskii and P.V. Chirnov, *Glass Phys. and Chem.* **6**, 239–43 (1980).

[25] G.W. Arnold and W.D. Compton, *Phys. Rev.* **116**, 802–11 (1959).

[26] G.H. Sigel, *J. Non-Cryst. Solids* **13**, 372–98 (1973/74).

[27] A.R. Ruffa, *J. Non-Cryst. Solids* **13**, 37–54 (1973/74).

[28] D.L. Griscom, E.J. Friebele and G.H. Sigel, "Observation and Analysis of the Primary ^{29}Si Hyperfine Structure of the E' Centre in Non-Crystalline SiO_2", *Solid State Commun.* **15**, 479–83 (1974).

[29] G. Hochstrasser and J.F. Antonini, "Surface States of Pristine Silica Surfaces 1. ESR Studies of E' Dargling Bonds and of CO_2 — Adsorbed Radicals", *Surface Sci.* **32**, 644–64 (1972).

[30] C.E. Jones and D. Embree, "Correlations of the 4.77–4.28 ev Luminescence Band in Silica with Oxygen Vacancy", *J. Appl. Phys.* **47**, 5365–71 (1976).

[31] E. Lell, N.J. Kreidl and J.R. Hensler, "Progress in Ceramic Science (Pergamon, London, 1966), vol. 4, p. 1.

[32] R.A. Weeks and E. Sonder, "Low Symposium on Paramagnetic Resonance" (Academic, New York, 1963), vol. 2, p. 869.

[33] R.A. Weeks, *Phys. Rev.* **130**, 570 (1963).

[34] F.J. Fiegl and J.H. Anderson, *J. Phys. Chem. Solids* **31**, 1575 (1970).

[35] E.W. Claffy, *Am. Mineral.* **38**, 919 (1953).

[36] A.T. Fujii and S. Isotani, *An. Acad. Bras. Ci.* **55**, 127 (1982).

[37] A.T. Fujii and S. Isotani, *An. Acad. Bras. Ci.* **60**, 127 (1988).

[38] S. Isotani, A.T. Fujii, R. Antonini, W.M. Pontuschka, S.R. Said and W.W. Furtado, *An. Acad. Bras. Ci.* **63**, 127 (1991).

[39] A.S. Ito and S. Isotani, *Rad. Ef. Def. Solids* **116**, 307 (1991).

[40] O.L. Dias, A.R.P.L. Albuquerque and S. Isotani, *An. Acad. Bras. Ci.* **55**, 173 (1983).

[41] K. Nassau and B.E. Prescott, *Am. Mineral.* **60**, 705 (1975).

[42] A.R.P.L. Albuquerque and S. Isotani, *Rad. Ef. Def. Solids* **106**, 143 (1988).

[43] J.J. Markham, *Rev. Mod. Phys.* **31**, 956 (1959).

[44] D.R. Hartree, "The Calculation of Atomic Structures", John Wiley & Sons Inc., New York (1957).

[45] M. Tinkham, "Group Theory and Quantum Mechanics", McGraw-Hill, New York (1964).

[46] S.Sasaki, K. Fujino, Y. Takeuchi and R. Sadanaga, *Acta Cryst.* **A36**, 904 (1980).

FIGURE CAPTIONS

Fig. 1. Optical absorption spectrum of annealed spodumene.

Fig. 2. Difference spectrum of lilac and bleached spodumene.

Fig. 3. Optical absorption spectra of γ-irradiated spodumene.

Fig. 4. Optical absorption spectra of irradiated and annealed topaz.

Fig. 5. Optical absorption spectra of natural and annealed-beryl.

Fig. 6. Optical absorption band scheme of silicates. Scale for $\Delta\overline{\nu}$ is five times small than $\overline{\nu}_0$ scale.

Fig. 7. Energy eigenvalues for single electron in polarized charge surface potential of radius R (see eq. 4).

Table I — Fit parameters of the optical absorption spectra of spodumene.

	$\overline{\nu}_{oi}$	$\Delta\overline{\nu}_i$	absorbance				
line	(10^3 cm^{-1})	(10^3 cm^{-1})	annealed	difference	a	c	f
1	35.4	1.4	0.13	—	—	—	—
2	38.0	2.6	1.28	—	—	—	—
3	41.6	1.9	0.27	—	—	—	—
4	56.1	9.0	3.60	—	—	—	—
5	21.0	2.0	—	0.046	0.015	0.023	0.03
6	28.8	3.3	—	0.480	0.11	0.22	0.31
7	33.4	2.5	—	0.540	0.21	0.08	0.36
8	40.6	1.5	—	0.178	0.04	0.08	0.115
9	43.7	2.8	—	0.828	0.27	0.42	0.54
10	47.5	1.2	—	0.460	0.15	0.23	0.30
11	15.6	2.0	—	—	0.03	0.046	0.06
12	18.6	1.0	—	—	0.03	0.03	0.03

Table II — Fit parameters of the optical absorption spectra of topaz.

$\overline{\nu}_{oi}$ (10^3 cm^{-1})	$\Delta\overline{\nu}_i$ (10^3 cm^{-1})	Irradiated	Heated at 200°C	Heated at 600°C
21.0	4.5	0.13	—	—
28.0	4.0	0.09	—	—
34.0	3.5	0.23	0.03	—
38.0	1.6	0.18	0.10	—
41.0	2.6	0.47	0.37	0.37
44.4	1.9	0.17	0.14	0.13
47.5	2.5	0.10	—	—
57.0	10.0	0.75	0.62	0.67

Table III — Fit parameters of the optical absorption spectra of beryl.

$\overline{\nu}_{oi}$ (10^3 cm^{-1})	$\Delta\overline{\nu}_i$ (10^3 cm^{-1})	Natural	Heated at 750°C
35.2	1.8	0.18	0.09
37.4	1.5	0.18	0.11
41.0	2.6	0.54	0.34
43.5	2.7	0.28	0.19
61.0	10.5	3.80	2.80

Table IV — Fit parameters of the optical absorption spectra of quartz.

$\overline{\nu}_{oi}$ (10^3 cm^{-1})	$\Delta\overline{\nu}_i$ (10^3 cm^{-1})	quartz
20.2	2.4	0.05
27.4	3.2	0.07
35.1	4.1	0.15
43.6	4.0	0.54
46.6	1.1	0.04
51.1	3.2	0.21
59.9	5.7	0.79

Table V

symmetry	orbital	representation
C_{1v}	s	$\Gamma(s) = A'$
	p	$\Gamma(p) = A' + A' + A''$
C_{2v}	s	$\Gamma(s) = A_1$
	p	$\Gamma(p) = A_1 + B_1 + B_2$
C_1	s	$\Gamma(s) = A$
	p	$\Gamma(p) = A + A + A$

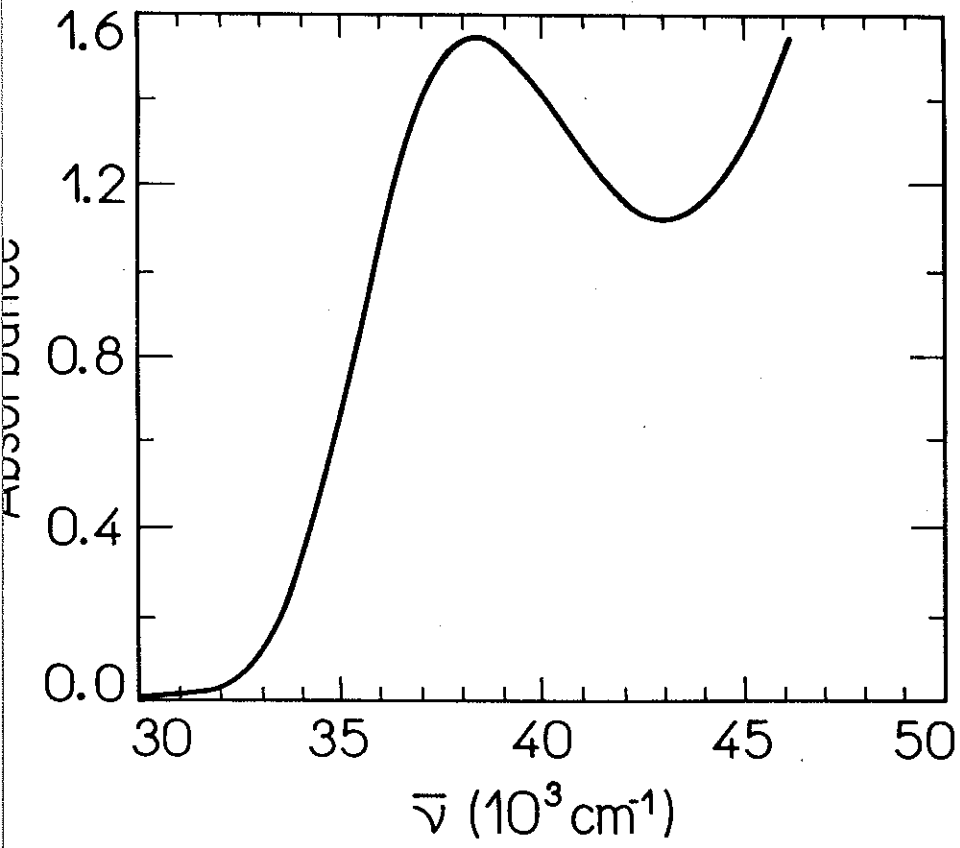

fig 1

Phys. Review
Oxygen vacancy . . . I
S. Isotani et al

Fig 1

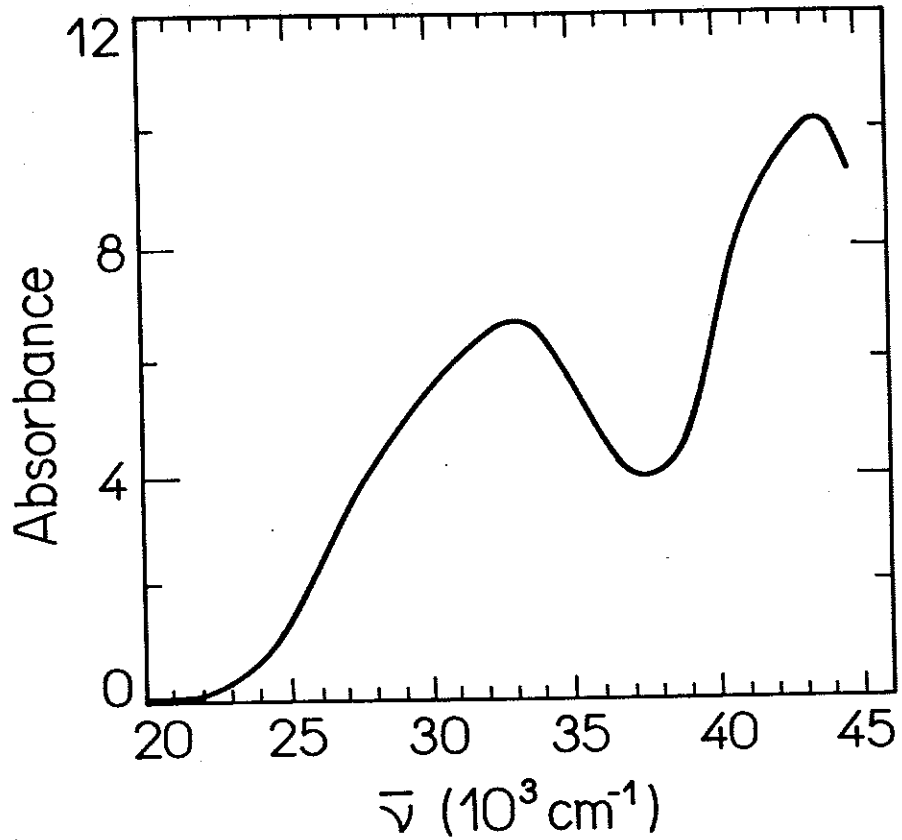

fig

Phys. Review
Oxygen vacancy . . . I.

Fig 2

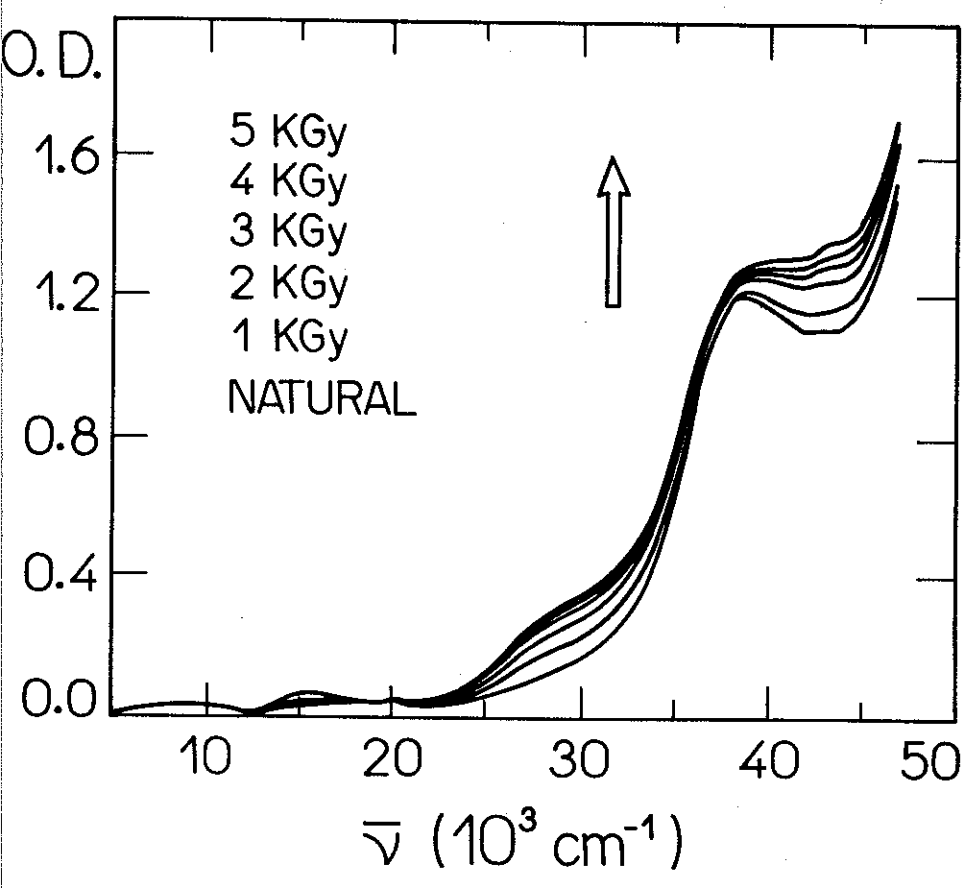

Fig 3

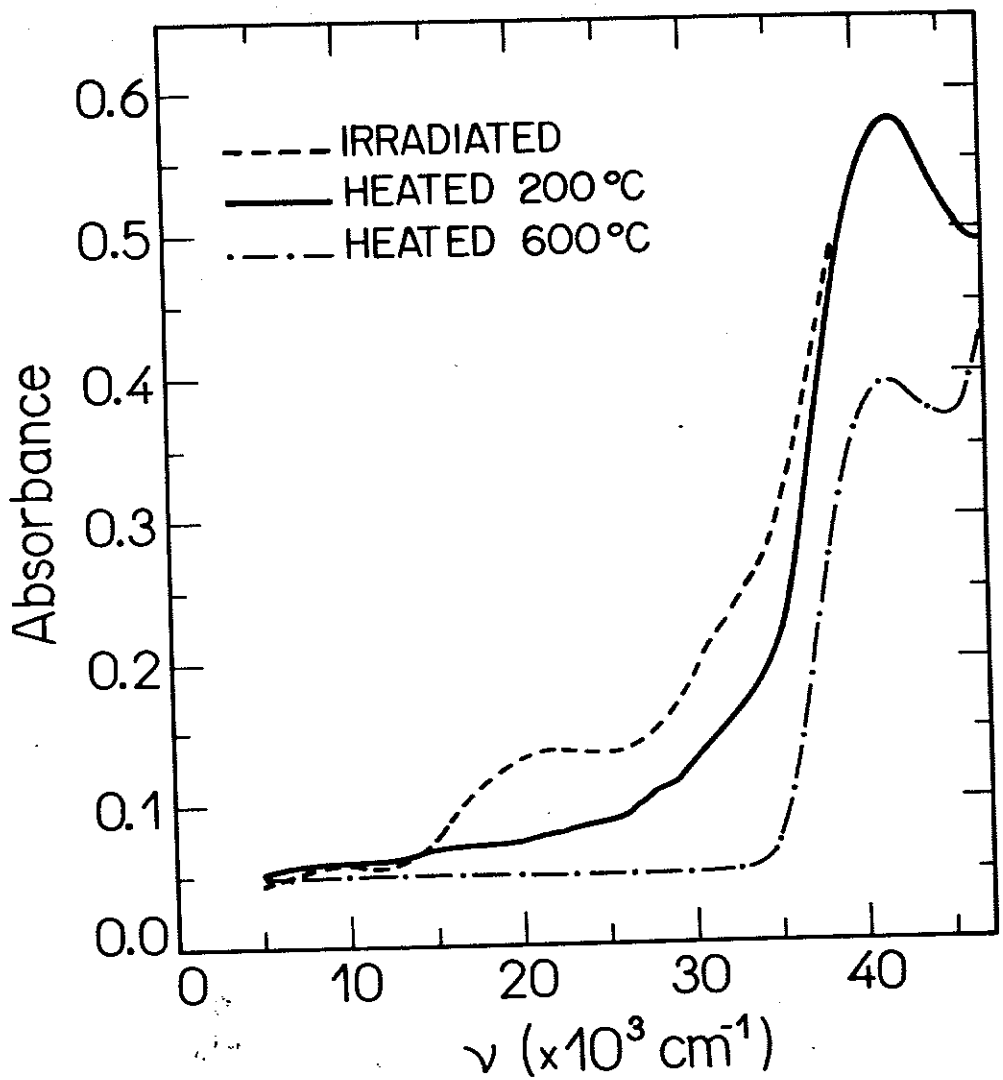

Phys. Rev.
Oxygen vacancy . . . I Fig 3
S Isotani et al

Phys. Rev.
Oxygen vacancy . . . I Fig 4

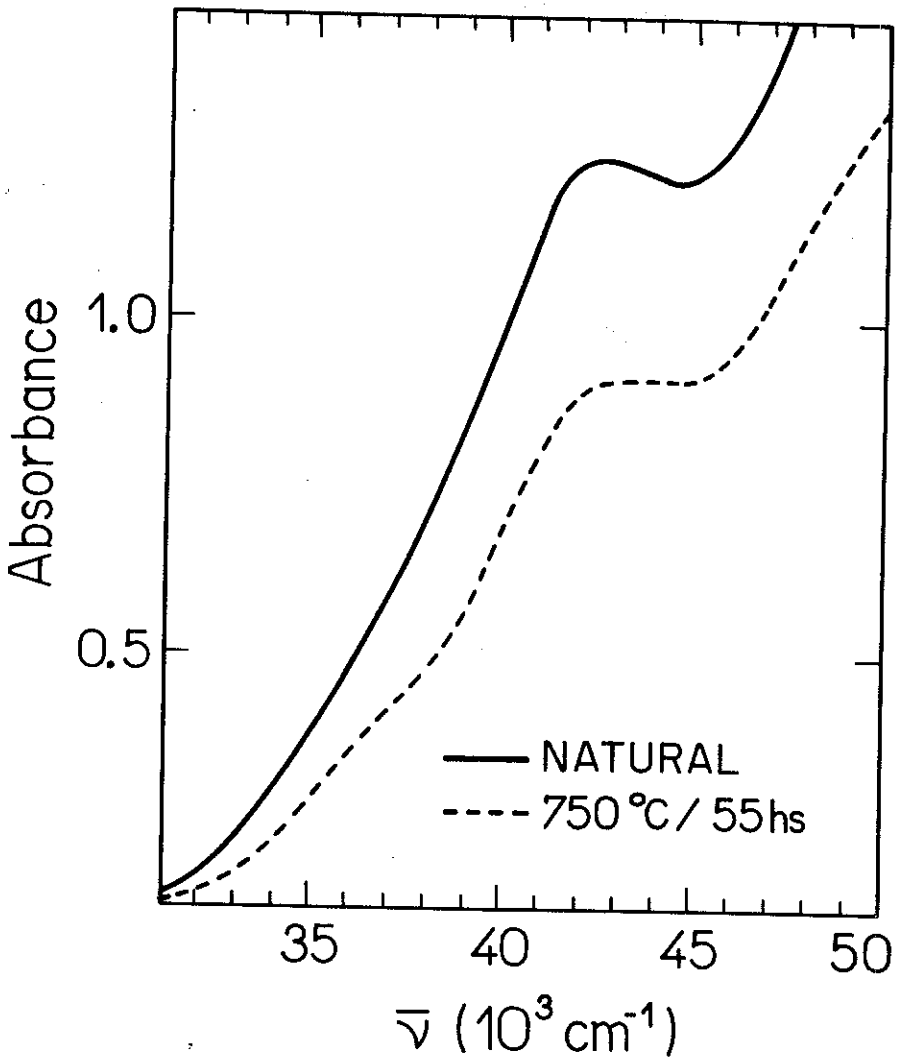

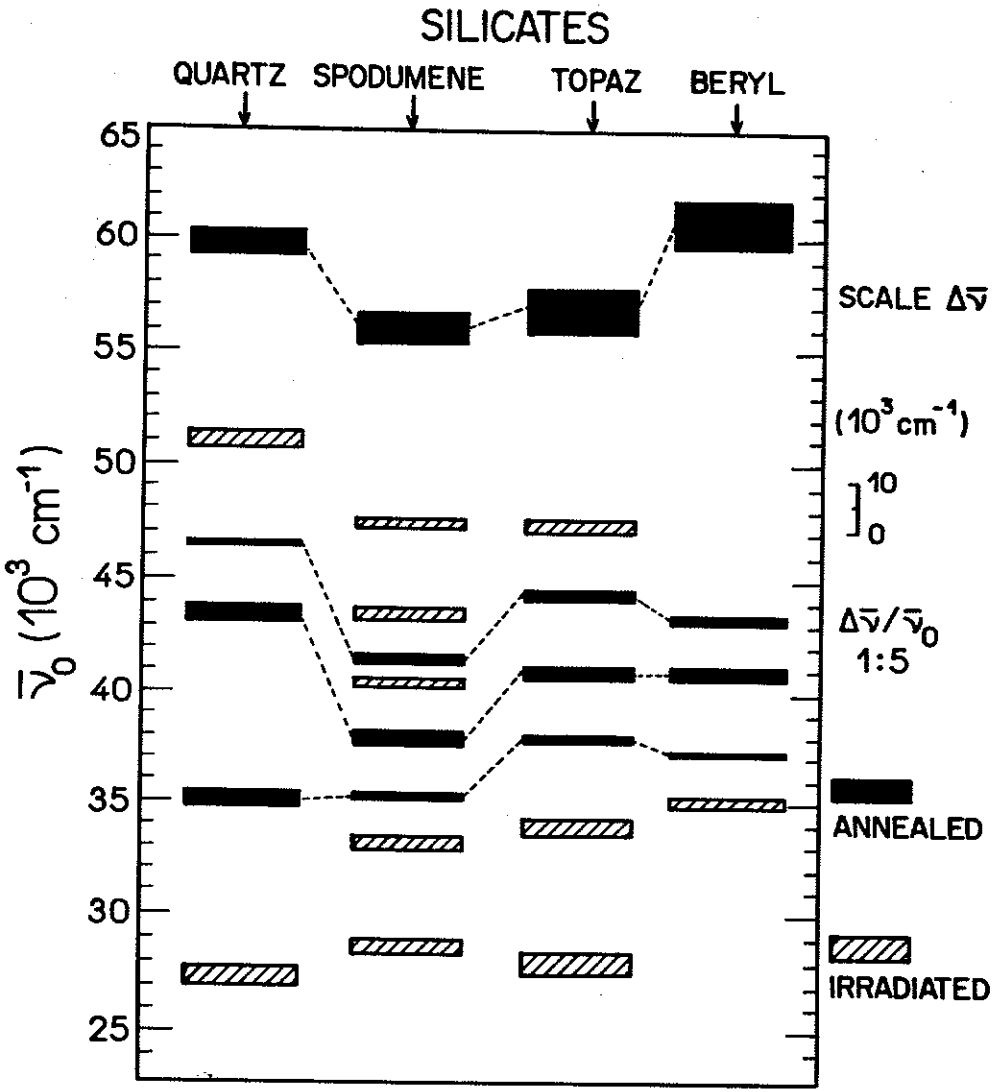

Phys. Rev.
Oxygen vacancy ... J. Fe 5

Phys. Rev.
Oxygen vacancy ... J. Fe 6

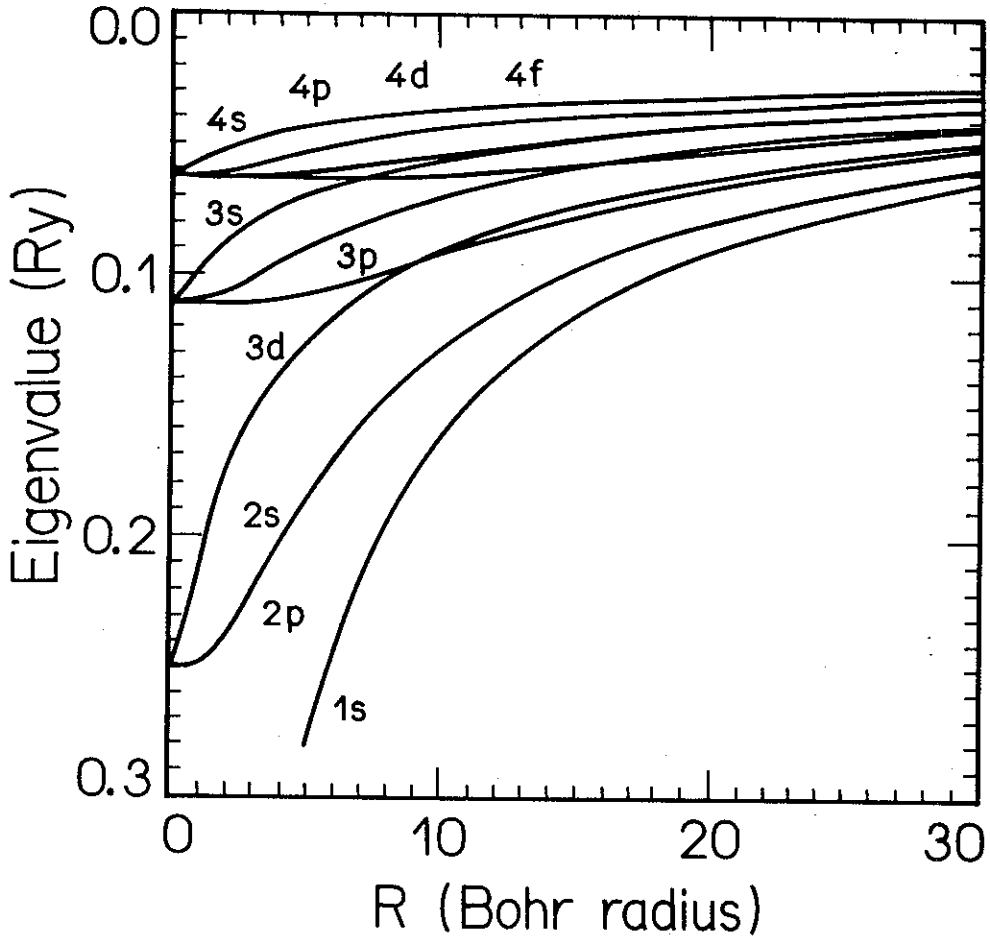

Phys. Rev.
Oxygen vacancy Fig 7
S. Isotani et al